Centrum voor Wiskunde en Informatica

REPORT*RAPPORT*

MAS

Modelling, Analysis and Simulation

Modelling, Analysis and Simulation

Two-level Fourier analysis of a multigrid approach for discontinuous Galerkin discretisation

P.W. Hemker, W. Hoffmann, M.H. van Raalte

REPORT MAS-R0206 APRIL 30, 2002

CWI is the National Research Institute for Mathematics and Computer Science. It is sponsored by the Netherlands Organization for Scientific Research (NWO).
CWI is a founding member of ERCIM, the European Research Consortium for Informatics and Mathematics.

CWI's research has a theme-oriented structure and is grouped into four clusters. Listed below are the names of the clusters and in parentheses their acronyms.

Probability, Networks and Algorithms (PNA)

Software Engineering (SEN)

Modelling, Analysis and Simulation (MAS)

Information Systems (INS)

P.O. Box 94079, 1090 GB Amsterdam (NL)
Kruislaan 413, 1098 SJ Amsterdam (NL)
Telephone +31 20 592 9333
Telefax +31 20 592 4199

ISSN 1386-3703

Two-Level Fourier Analysis of a Multigrid Approach for Discontinuous Galerkin Discretisation

P.W. Hemker[*,**], W. Hoffmann[**] and M.H. van Raalte[*,**]

[*] *CWI, P.O. Box 94079, 1090 GB Amsterdam, The Netherlands*

[**] *KdV Institute for Mathematics, University of Amsterdam*
Plantage Muidergracht 24, 1018 TV Amsterdam, The Netherlands

ABSTRACT

In this paper we study a multigrid method for the solution of a linear second order elliptic equation, discretized by discontinuous Galerkin (DG) methods, and we give a detailed analysis of the convergence for different block-relaxation strategies.

We find that point-wise block-partitioning gives much better results than the classical cell-wise partitioning. Both for the Baumann-Oden and for the symmetric DG method, with and without interior penalty, the block relaxation methods (Jacobi, Gauss-Seidel and symmetric Gauss-Seidel) give excellent smoothing procedures in a classical multigrid setting. Independent of the mesh size, simple MG cycles give convergence factors 0.075 – 0.4 per iteration sweep for the different discretisation methods studied.

2000 Mathematics Subject Classification: 65F10, 65N12, 65N15, 65N30, 65N55
Keywords and Phrases: Discontinuous Galerkin method, multigrid iteration, two-level Fourier analysis, point-wise block-relaxation

1. Introduction

Although discontinuous Galerkin (DG) methods are traditionally used for the solution of hyperbolic equations [8, 16, 19], recently new interest arises for application to elliptic problems. Early methods for elliptic problems [9, 17] were considered unattractive because they result in discrete systems that show a saddle-point problem behavior: The non-definite spectrum makes time-stepping procedures unstable and many iterative methods inadequate for the computation of steady solutions. The fix by introducing an interior penalty (IP) to penalize the discontinuity in the discrete solution [2, 20, 22] is effective, but leaves the user with the quite arbitrary choice of an $\mathcal{O}(h^{-1})$ penalty parameter.

In 1998 Baumann-Oden [5, 6, 18] published another stable method of DG type without such a free parameter. This interesting method, however, results in an asymmetric discrete operator, even for the discretisation of a symmetric continuous problem. In this paper we consider the asymmetric (Baumann) and the symmetric discretisation method, both with

and without interior penalty. For an excellent survey and a unified analysis of the different DG methods for elliptic problems we refer to [3].

The motivation for our present research is our interest in the *hp*-self-adaptive solution of three-dimensional problems of convection-diffusion type on a dyadic grid. Here DG methods are particularly attractive because of their ability to handle conveniently difficulties related to order- and grid-adaptation [15, 21]. For the solution of the resulting discrete systems we want to rely on multigrid (MG) methods because of their expected optimal efficiency. The framework of the combined adaptive discretisation and the multigrid solution process is found, e.g., in [7, 13]. The basic idea is summarized in Section 2.4 below.

We emphasize that our approach is quite different from the analysis of MG as preconditioner, analyzed for DG methods by [10]. Considering MG as an independent solution process gives us the opportunity not only to solve a linear system but to simultaneously create the adaptive grid together with solving the discrete (linear) system. This use of MG allows us to drop the CG iteration, preserving the optimal $\mathcal{O}(N)$ property [11]. Moreover, the local mode analysis allows us to study not only the symmetric positive definite case, but also the asymmetric and non-penalized methods.

In this paper we study the convergence of the MG method by smoothing analysis and by analyzing the two-level convergence behavior, restricting ourselves to the discretized Poisson equation in one space dimension. With considerably extra complexity the same analysis can be made for two or three space dimensions, but it is not expected that such results will be essentially different.

We show that the discrete operator can be partitioned in block-tridiagonal form in two essentially different ways: *cell-wise* and *point-wise*. For each of these partitionings, block-relaxation methods (block Jacobi, block Gauss-Seidel) can be used as a smoothing procedure in the MG algorithm. It appears that the type of block-partitioning makes an essential difference: the pointwise block-partitioning shows a much better convergence than the usual cell-wise block-partitioning. It appears that pointwise block-partitioning even leads to good smoothing for the symmetric DG-method of saddle-point type.

The outline of this paper is as follows. In Section 2 we describe the DG discretizations used. We select a particular basis in the space of piecewise polynomial functions for the test- and trial space, in order to introduce the distinction between cell- and point-wise block partitionings. We show the MG algorithm and describe in detail the grid-transition operators used.

In Section 3 we develop the Fourier analysis tools needed to make the local mode analysis for the block-Toeplitz matrices: the discretisation operator, the prolongation and the restriction operator. Then, in Section 4 we apply the smoothing analysis to the cell- and point-wise partitioned discretisation. We determine the smoothing factors and compute optimal damping parameters. The results motivate us to continue with the two-level analysis for the point-wise partitioning exclusively. Therefore, in Section 5 we take the MG coarse-grid-correction into account. We compute the spectral radii for the error reduction operators and we compute optimal damping parameters for the two-level algorithm. It appears that an error reduction factor of 0.075 (for symmetric Gauss-Seidel) to 0.4 (for damped Jacobi) per MG-sweep is predicted for the non-penalized discretizations. For the penalized method the convergence is somewhat slower, but still faster than 0.6 per MG-sweep. In order to see what can be the worst possible behavior in a single or a couple of iteration sweeps, we also

compute the corresponding spectral norms. We conclude that MG converges rapidly in all cases.

In Section 6 we show by Fourier analysis the consistency and the convergence of the discretisation stencils obtained by the DG methods. This gives some additional insight in the accuracy of the different methods and in the lack of adjoint consistency of Baumann's method as signaled in [3]. In the final section we show some numerical results that illustrate the analyzed behavior and show the fast convergence of the MG method.

2. The discontinuous Galerkin Discretisation

2.1 Discontinuous Galerkin methods

In order to describe the discretisation method studied in this paper, we first give the special weak form of the equation as used for these discontinuous Galerkin (DG) discretisation methods. On a cube Ω we consider the Poisson equation, partly with Neumann and partly with Dirichlet boundary conditions:

$$-\nabla \cdot \nabla u = f \text{ on } \Omega; \quad u = u_0 \text{ on } \Gamma_{\mathrm{D}} \cap \partial\Omega, \quad u_n = g \text{ on } \Gamma_N \cap \partial\Omega.$$

On Ω we introduce a uniform partitioning Ω_h, i.e., a set of disjoint rectangular cells in Ω, all of identical shape:

$$\Omega_h = \left\{ \Omega_e \;\middle|\; \cup_e \Omega_e = \Omega,\ \Omega_i \cap \Omega_j = \emptyset,\ i \neq j \right\}.$$

We define on Ω_h the *broken Sobolev space* [6, 18, 4] for non-negative integer k,

$$H^k(\Omega_h) = \left\{ u \in L_2(\Omega) \,\middle|\, u|_{\Omega_e} \in H^k(\Omega_e), \quad \forall \Omega_e \in \Omega_h \right\}.$$

Then, the weak form of the equation, associated with the DG-methods, reads [6, 18]: find $u \in H^1(\Omega_h)$ such that:

$$B(u,v) = L(v) \quad \forall v \in H^1(\Omega_h), \tag{2.1}$$

where

$$\begin{aligned} B(u,v) = &\sum_{\Omega_e \in \Omega_h} \int_{\Omega_e} \nabla u \cdot \nabla v dx - \int_{\Gamma_{\mathrm{int}} \cup \Gamma_{\mathrm{D}}} \langle \nabla u \rangle \cdot [v]\, ds \\ &+ \sigma \int_{\Gamma_{\mathrm{int}} \cup \Gamma_{\mathrm{D}}} \langle \nabla v \rangle \cdot [u]\, ds + \mu \int_{\Gamma_{\mathrm{int}} \cup \Gamma_{\mathrm{D}}} [u] \cdot [v]\, ds, \end{aligned} \tag{2.2}$$

and

$$L(v) = \sum_{\Omega_e \in \Omega_h} \int_{\Omega_e} f v\, dx + \sigma \int_{\Gamma_{\mathrm{D}}} \langle \nabla v \rangle \cdot [u_0]\, ds + \int_{\Gamma_N} g v\, ds.$$

Here Γ_{int} is the union of all interior cell faces, and $\sigma \neq 0$ and $\mu > 0$ are parameters identifying the different DG methods. ($\sigma = 1$ for Baumann's method; $\sigma = -1$ for symmetric DG; $\mu > 0$

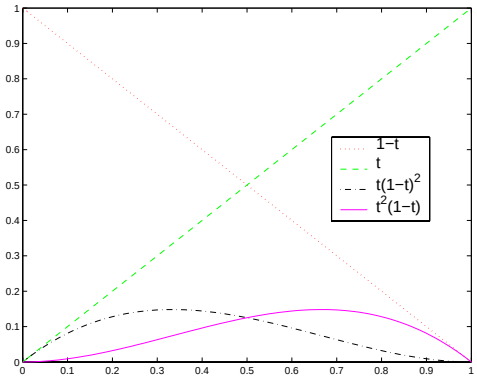

Figure 1: $\phi_{n,k}(t) = t^{n+k}(1-t)^{n+1-k}$, $n = \{0,1\}$, $\quad k = \{0,1\}$.

the interior penalty parameter.) The jump operator $[\cdot]$ and the average operator $<\cdot>$ are defined at the common interface $\Gamma_{i,j}$ between two adjacent[1] cells Ω_i and Ω_j by

$$\begin{aligned} [w(x)] &= w(x)|_{\partial\Omega_i}\mathbf{n}_i + w(x)|_{\partial\Omega_j}\mathbf{n}_j, \\ \langle w(x)\rangle &= \frac{1}{2}\left(w(x)|_{\partial\Omega_i} + w(x)|_{\partial\Omega_j}\right), \end{aligned} \tag{2.3}$$

for $x \in \Gamma_{i,j} \subset \Gamma_{\text{int}}$. Here $\mathbf{n}_i$ is the unit outward pointing normal for cell Ω_i. In case of a vector valued function, τ, we define

$$\begin{aligned} [\tau(x)] &= \tau(x)|_{\partial\Omega_i}\cdot\mathbf{n}_i + \tau(x)|_{\partial\Omega_j}\cdot\mathbf{n}_j, \\ \langle \tau(x)\rangle &= \frac{1}{2}\left(\tau(x)|_{\partial\Omega_i} + \tau(x)|_{\partial\Omega_j}\right). \end{aligned} \tag{2.4}$$

The DG discretisation is obtained by specifying the finite-dimensional trial and test space $S_h \subset H^1(\Omega_h)$ as the space of piecewise polynomials of degree less than $2p$ on the partitioning Ω_h:

$$S_h = \left\{\phi_{i,e} \in P^{2p-1}(\Omega_e), \quad \Omega_e \in \Omega_h\right\}.$$

Notice that we restrict ourselves to odd degree $k = 2p-1$. The discrete equations now read: find $u_h \in S_h$ such that

$$B(u_h, v_h) = L(v_h) \qquad \forall v_h \in S_h\,. \tag{2.5}$$

2.2 Choice of a basis

To completely describe the discrete matrix obtained, we should provide S_h with a basis. Therefore we introduce the following basis polynomials on the one-dimensional unit interval

$$\phi_{2n+k}(t) = t^{n+k}(1-t)^{n+1-k}, \quad n = 0,1,\cdots,p-1, \quad k = 0,1. \tag{2.6}$$

[1] At a Dirichlet boundary the interface with a virtual (flat, exterior) adjacent cell, containing only the Dirichlet data, is used.

On the unit cube, $\hat{\Omega} \subset \mathbb{R}^d$, we use a basis of tensor-product polynomials based on (2.6). A basis for $P^{2p-1}(\Omega_e)$ is obtained by the usual affine mapping $\widehat{\Omega} \to \Omega_e$.

The basis thus obtained has two advantages. First of all it is hierarchical. This means that we can (locally) increase the accuracy of the approximation just by extending the basis with higher order polynomials[2]. Secondly, the coefficients of the first degree polynomials represent function values at the cell-corners, while the coefficients of the polynomials of degree three can be associated with corrections for the derivatives at the cell corners. All higher order polynomials are genuine bubble functions and correspond to interior cell corrections only.
If we are interested in fast convergence of the solution procedure for the discrete system, the coefficients for these bubble functions are of less importance because they can be eliminated by static condensation or they can be dealt with by defect correction. Therefore, in our analysis in the following sections we restrict ourselves to the case $p = 2$. Furthermore, we restrict ourselves to the one-dimensional equation, because this is the essential building block for the higher-dimensional case where we use tensor product[3] polynomials.

Using the basis $\{\phi_i\}_{i=0}^3$, the approximate solution reads

$$u_h = \sum_{e=1}^{N} \sum_{i=0}^{3} c_{i,e} \phi_i((x - x_e)/h) \equiv \sum_{e=1}^{N} \sum_{i=0}^{3} c_{i,e} \phi_{i,e}(t) ,$$

and we obtain the explicit form of the discrete system, $L_h u_h = f_h$,

$$\begin{aligned} \sum_{e=1}^{N} \sum_{i=0}^{3} c_{i,e} \Big(& \int_{\Omega_e} \phi'_{i,e}(x) \phi'_{j,e}(x) dx - \left\langle \phi'_{i,e}(x) \right\rangle \cdot [\phi_{j,e}(x)] \,|_{\Gamma_{\mathrm{Dint}}} + \\ & \sigma \, [\phi_{i,e}(x)] \cdot \left\langle \phi'_{j,e}(x) \right\rangle |_{\Gamma_{\mathrm{Dint}}} + \mu \, [\phi_{i,e}(x)] \cdot [\phi_{j,e}(x)] \,|_{\Gamma_{\mathrm{Dint}}} \Big) = \\ \sum_{e=1}^{N} \sum_{i=0}^{3} & \int_{\Omega_e} f \phi_{j,e}(x) dx + \sigma \, [u_0] \cdot \left\langle \phi'_{j,e}(x) \right\rangle |_{\Gamma_{\mathrm{D}}} + g \phi_{j,e}(x)|_{\Gamma_N} , \end{aligned} \tag{2.7}$$

for $4N$ test functions $\phi_{j,e}$. As usual, the resulting 1D discrete operator has a block-tri-diagonal structure. We want to emphasize that for solving this discrete system by block-relaxation we can follow two distinct approaches. The usual approach is to order the basis functions *cell-wise*. Then the choice of a particular basis for the polynomial space is of less importance and the variables in each block are associated with the coefficients of the polynomial approximation in the corresponding cell. The other approach is by ordering the coefficients *point-wise* and to associate with each point the left- and the right-sided value of the function and its derivative. (In fact, this motivates the particular choice of our basis (2.6).)

[2] A slightly better alternative basis satisfying our purposes is, defined on [-1,+1], the basis: $(x-1)^p(x+1)^q$, with $(p,q) = (1,0),\ (0,1),\ (2,1),\ (1,2)$, and $(x-1)^2(x+1)^2 P_n^{(2,2)}(x)$, with $n = 0, 1, \cdots$, and $P_n^{(2,2)}$ the Jacobi polynomials [1, p.774]. The first four polynomials in this basis are essential for our purpose, because they represent function values and first derivatives at the cell boundaries. The higher order polynomials satisfy a useful orthogonality property. This basis also relieves the restriction to odd degree k for $k > 4$.

[3] Notice that for higher order accuracy not *all* tensor product basis functions have to be included. Higher order cross-products of total degree higher than $2p-1$ can be neglected. This gives a significant reduction of computational work. (In two dimensions asymptotically a factor 2, in three dimensions a factor 6.)

Ordering the equations (the weighting functions $\phi_{e,j}$) and coefficients *cellwise* as $[c_{e,0}, c_{e,1}, c_{e,3}, c_{e,2}]$, yields the following discretisation stencil:

$$\left[\begin{array}{cccc|cccc|cccc} -\frac{1}{2} & 0 & -\frac{1}{2} & \frac{1-\sigma}{2}-h\mu & \frac{1+\sigma}{2}+h\mu & \frac{1}{2} & 0 & \frac{-1-\sigma}{2} & \frac{1}{2}\sigma & 0 & 0 & 0 \\ 0 & 0 & 0 & \frac{1}{2}\sigma & -\frac{1}{2}\sigma & \frac{2}{15} & \frac{1}{30} & 0 & 0 & 0 & 0 & 0 \\ 0 & 0 & 0 & 0 & 0 & \frac{1}{30} & \frac{2}{15} & -\frac{1}{2}\sigma & \frac{1}{2}\sigma & 0 & 0 & 0 \\ 0 & 0 & 0 & \frac{1}{2}\sigma & \frac{-1-\sigma}{2} & 0 & \frac{1}{2} & \frac{1+\sigma}{2}+h\mu & \frac{1-\sigma}{2}-h\mu & -\frac{1}{2} & 0 & -\frac{1}{2} \end{array}\right]. \tag{2.8}$$

If we order the equations and coefficients *pointwise*, according to function values and corrections on derivatives at the cell-interfaces, $[c_{e-1,3}, c_{e-1,2}, c_{e,0}, c_{e,1}]$, we get the stencil:

$$\left[\begin{array}{cccc|cccc|cccc} 0 & 0 & 0 & \frac{1}{30} & \frac{2}{15} & -\frac{1}{2}\sigma & \frac{1}{2}\sigma & 0 & 0 & 0 & 0 & 0 \\ 0 & \frac{1}{2}\sigma & \frac{-1-\sigma}{2} & 0 & \frac{1}{2} & \frac{1+\sigma}{2}+h\mu & \frac{1-\sigma}{2}-h\mu & -\frac{1}{2} & 0 & -\frac{1}{2} & 0 & 0 \\ 0 & 0 & -\frac{1}{2} & 0 & -\frac{1}{2} & \frac{1-\sigma}{2}-h\mu & \frac{1+\sigma}{2}+h\mu & \frac{1}{2} & 0 & \frac{-1-\sigma}{2} & \frac{1}{2}\sigma & 0 \\ 0 & 0 & 0 & 0 & 0 & \frac{1}{2}\sigma & -\frac{1}{2}\sigma & \frac{2}{15} & \frac{1}{30} & 0 & 0 & 0 \end{array}\right]. \tag{2.9}$$

For the Poisson equation on the uniform grid, in both cases the discretisation matrix appears to be a block-Toeplitz matrix. This matrix is described by the repetition of either stencil (2.8) or stencil (2.9).

2.3 Restrictions and prolongations

As we are interested in multigrid methods for the solution of the discrete equations arising from discontinuous Galerkin discretisation, we need proper restriction and prolongation operators. With piecewise polynomial approximations on the separate cells of the partitioning Ω_h, a natural prolongation is immediately derived. For convenience we describe the grid transition operators for the one-dimensional case. Extension to higher dimensions follows immediately by means of the tensor product principle.

We consider a fine partitioning Ω_h and a coarse partitioning Ω_H, with $H = 2h$ and with nodal points jh and jH respectively, and we denote the spaces of discontinuous piecewise polynomials by S_h and S_H. It is immediately clear that $S_H \subset S_h$. This defines the natural prolongation $P_{hH} : S_H \to S_h$ so that $(P_{hH}u_H)(x) = u_H(x)$ for all $x \in \mathbb{R} \setminus \mathbb{Z}_h$.[4] Given a polynomial basis, this prolongation is explicitly described by its stencil. For our basis $\{\phi_{i,e}\}$ the stencil reads

$$P_{hH} \approxeq \left[\begin{array}{cccc|cccc|cccc|cccc} 0 & 0 & 0 & \frac{-1}{8} & 0 & 0 & 0 & \frac{1}{4} & \frac{3}{8} & 0 & 0 & 0 & 0 & 0 & 0 & 0 & 0 & 0 & 0 & 0 \\ 0 & 0 & 0 & 0 & 0 & 0 & \frac{1}{2} & \frac{1}{8} & 0 & 1 & 0 & 0 & \frac{1}{8} & \frac{1}{2} & 0 & 0 & 0 & 0 & 0 & 0 \\ 0 & 0 & 0 & 0 & 0 & 0 & \frac{1}{2} & \frac{1}{8} & 0 & 0 & 1 & 0 & \frac{1}{8} & \frac{1}{2} & 0 & 0 & 0 & 0 & 0 & 0 \\ 0 & 0 & 0 & 0 & 0 & 0 & 0 & 0 & 0 & 0 & 0 & \frac{3}{8} & \frac{1}{4} & 0 & 0 & 0 & \frac{-1}{8} & 0 & 0 & 0 \end{array}\right].$$

Different from the prolongation, a natural restriction is not uniquely determined. However, we recognize a natural restriction for the residue, associated with the weighted-residual character of the Galerkin discretisation. This restriction is the adjoint of the natural prolongation. I.e., the Toeplitz operator for this restriction is the transposed of the Toeplitz operator for the natural prolongation. We denote this restriction as $\overline{R}_{Hh} = (P_{hH})^T$. It follows from the Galerkin construction of the discretisation and from the nesting of the spaces S_h and S_H, that the Galerkin relation exists between the discretisation on the coarse and the finer grid,

$$L_H = \overline{R}_{Hh} L_h P_{hH} \ . \tag{2.10}$$

[4] $\mathbb{Z}_h$ is the infinite regular one-dimensional grid, defined by $\mathbb{Z}_h = \{jh \,|\, j \in \mathbb{Z}, h > 0\}$.

Associated with the chosen basis $\{\phi_{i,e}\}$, which is essentially based on the function values and corrections for the derivatives at the cell endpoints, we can construct another pointwise restriction (the injective restriction). This restriction is constructed such that

$$\begin{aligned}(d/dx)(R_{Hh}u_h)(jH)|_{\Omega_{H,j-1}} &= (d/dx)u_h(2jh)|_{\Omega_{h,2j-1}}\,,\\ (R_{Hh}u_h)(jH)|_{\Omega_{H,j-1}} &= u_h(2jh)|_{\Omega_{h,2j-1}}\,,\\ (R_{Hh}u_h)(jH)|_{\Omega_{H,j}} &= u_h(2jh)|_{\Omega_{h,2j}}\,,\\ (d/dx)(R_{Hh}u_h)(jH)|_{\Omega_{H,j}} &= (d/dx)u_h(2jh)|_{\Omega_{h,2j}}\,.\end{aligned}$$

The stencil related with this restriction reads

$$R_{Hh} \approxeq \left[\begin{array}{cccc|cccc|cccc|cccc|cccc} 0&0&0&1&0&0&0&0&3&0&0&0&0&0&0&0&0&0&0&0\\ 0&0&0&0&0&0&0&0&0&1&0&0&0&0&0&0&0&0&0&0\\ 0&0&0&0&0&0&0&0&0&0&1&0&0&0&0&0&0&0&0&0\\ 0&0&0&0&0&0&0&0&0&0&0&3&0&0&0&0&1&0&0&0 \end{array}\right].$$

We see that the prolongation P_{hH} and this restriction R_{Hh} satisfy the relation $R_{Hh}P_{hH} = I_H$, i.e., the identity operator on S_H. This implies that the operator $P_{hH}R_{Hh}$ is a projection operator from S_h into itself. Its image, $\mathrm{Range}(P_{hH}) \subset S_h$ are the *fine grid functions representable* on the coarse grid. So is the range of the complementary projection $I_h - P_{hH}R_{Hh}$, the set of *fine grid functions* that are *not representable* on the coarse grid.

2.4 The multigrid algorithm

Our main interest lies in the application of the DG method in the *hp*-self-adaptive multigrid algorithm. Therefore we describe this algorithm [13], where local refinements yield corrections for the coarser dicretisations, in a general form. Whereas the final application will be for three-dimensional problems, where the combination of an efficient discretisation and a fast solution algorithm is of utmost importance, in the sections that follow we restrict ourselves to the analysis of the one-dimensional multigrid solution process.

The adaptive algorithm starts at refinement level (0) and in a recursive way it introduces (locally) finer cells on the higher levels, by refinement of the current (partial) grid. In this way a regular family of nested refinements is obtained.

Given on the i-th refinement level the discrete operator L_H and discrete right-hand side f_H, on level i we also choose a first approximation to the solution u_H . E.g., in the linear case on the coarsest grid we may choose $u_H = 0$. Furthermore, we start with the current approximation of the truncation error $\tau_H = 0$ on level i.

The adaptive multilevel algorithm (AMLA) simultaneously solves the discrete equations and introduces refinements where needed.
On level i the algorithm AMLA consists of the following steps [13]:

1. relax the discrete system

   $$L_H\, u_H = f_H + \tau_H\,,$$

   by ν_2 sweeps of a relaxation procedure;

2. **if** adaptation of grid or order is needed **then**

– determine (locally) the order of approximation (optional);
– remove or create (locally) finest cells where needed;
– determine (locally) the fine grid operator, L_h, and the right-hand side, f_h, and set $\tau_h = 0$;
– determine an approximation of the solution on the finer grid *by interpolation* $u_h = P_{hH} u_H$;

endif;

3. apply one step of AMLA to level $i+1$ for the solution of

$$L_h u_h = f_h + \tau_h \,;$$

4. compute the relative truncation error at level i

$$\tau_H := (L_H R_{Hh} - \overline{R}_{Hh} L_h) u_h \,;$$

5. relax

$$L_H \, u_H = f_H + \tau_H \,,$$

by ν_1 sweeps of a relaxation procedure.

In the linear case, if the total grid is refined, the algorithm corresponds with the classical multigrid [11], combined with nested iteration. Its convergence is best studied by means of the two-level algorithm. The amplification operator of the error is given by

$$M_h^{\mathrm{TLA}} = (M_h^{\mathrm{REL}})^{\nu_2} M_h^{\mathrm{CGC}} (M_h^{\mathrm{REL}})^{\nu_1} \,, \tag{2.11}$$

ν_1 and ν_2 are the number of pre- (post-) relaxation sweeps respectively, and

$$M_h^{\mathrm{CGC}} = I_h - P_{hH} L_H^{-1} \overline{R}_{Hh} L_h \,.$$

With each of the amplification operators of the error, M_h, corresponds an amplification operator for the residue $\overline{M}_h = L_h M_h L_h^{-1}$. In our analysis we are mainly interested in the convergence of the two-level iteration. Therefore we compute the spectral radius of the amplification operator $\rho(M_h^{\mathrm{TLA}}) = \rho(\overline{M}_h^{\mathrm{TLA}})$, which represents the final convergence factor per iteration step. We also compute the spectral norms $\|(M_h^{\mathrm{TLA}})^t\|_2$ and $\|(\overline{M}_h^{\mathrm{TLA}})^t\|_2$ which describe the worst possible convergence rate in t steps.

3. Fourier analysis tools

3.1 Fourier analysis for vector grid functions

In order to apply Fourier analysis methods for the convergence study of our solution process, we introduce some elementary tools. We first introduce (vector valued) grid functions defined on the regular, unbounded one-dimensional grid

$$\mathbb{Z}_h = \{ jh \,|\, j \in \mathbb{Z}, h > 0 \} \,.$$

The Hilbert space of square summable scalar grid functions, defined on $\mathbb{Z}_h$, with inner product

$$(u_h, v_h) = \sum_j h\, u_h(jh) v_h(jh)\,,$$

is denoted by $\ell^2(\mathbb{Z}_h)$. We will use the Fourier transform $\widehat{u_h}$ of $u_h \in l_h^2(\mathbb{Z}_h)$, which is the complex function defined on $\mathbb{T}_h = [-\pi/h, +\pi/h]$, defined by

$$\widehat{u_h}(\omega) = \frac{h}{\sqrt{2\pi}} \sum_{j\in\mathbb{Z}} e^{-ijh\omega}\, u_h(jh)\,. \tag{3.1}$$

The inverse transformation is given by

$$u_h(jh) = \frac{1}{\sqrt{2\pi}} \int_{\omega\in\mathbb{T}_h} e^{+ijh\omega}\, \widehat{u_h}(\omega)\, d\omega\,. \tag{3.2}$$

We see that the function $\widehat{u_h}(\omega)$ is $(2\pi/h)$-periodic, and that by Parseval's equality we have

$$\|u_h\|_{\ell^2(\mathbb{Z}_h)} = \|\widehat{u_h}\|_{L^2(\mathbb{T}_h)}\,. \tag{3.3}$$

In an obvious manner we can extend this definition of the Fourier transform $\ell^2(\mathbb{Z}_h) \to L^2(\mathbb{T}_h)$ to the Fourier transform of a four-dimensional vector function $u_h \in \left[\ell^2(\mathbb{Z}_h)\right]^4 \to \widehat{\mathbf{u}_h} \in \left[L^2(\mathbb{T}_h)\right]^4$.

The relations (3.1) and (3.2), as well as Parseval's equality (3.3) also hold if we replace u_h by the vector-valued gridfunction $\mathbf{u}_h \in \left[\ell^2(\mathbb{Z}_h)\right]^4$ and $\widehat{u_h}$ by $\widehat{\mathbf{u}_h} \in \left[L^2(\mathbb{T}_h)\right]^4$, provided that we use the corresponding norms for the vector spaces

$$\|\mathbf{u}_h\|^2_{[\ell^2(\mathbb{Z}_h)]^4} = \sum_{i=1}^4 \|u_{h,i}\|^2_{\ell^2(\mathbb{Z}_h)} \qquad \text{and} \qquad \|\widehat{\mathbf{u}_h}\|^2_{[L^2(\mathbb{T}_h)]^4} = \sum_{i=1}^4 \|\widehat{u_{h,i}}\|^2_{\mathbb{T}_h} \tag{3.4}$$

We apply this to the vector grid-functions of coefficients, either for the cell-centered (*cell-wise*) coefficients $u_h = \{[c_{e,0}, c_{e,1}, c_{e,3}, c_{e,2}]^T\}_{e\in\mathbb{Z}}$ or for the cell-corner (*pointwise*) coefficients $u_h = \{[c_{e-1,3}, c_{e-1,2}, c_{e,0}, c_{e,1}]^T\}_{e\in\mathbb{Z}}$. Cell-wise vector grid-functions are obtained from $H^2(\Omega_h)$ functions, with $\Omega = \mathbb{R}$, by the restriction operator $R^{\text{cell}}_{h,0} : H^2(\mathbb{R}_h) \to [\ell^2(\mathbb{Z}_h)]^4$ defined by

$$\begin{aligned}\mathbf{u}_h(jh) &= (R^{\text{cell}}_{h,0} u)(jh) = \\ &= \begin{bmatrix} & u((j-1)h)|_{\Omega_j} \\ h & u'((j-1)h)|_{\Omega_j} + u((j-1)h)|_{\Omega_j} - u(jh)|_{\Omega_j} \\ -h & u'(jh)|_{\Omega_j} - u((j-1)h)|_{\Omega_j} + u(jh)|_{\Omega_j} \\ & u(jh)|_{\Omega_j} \end{bmatrix},\end{aligned} \tag{3.5}$$

where $u(jh)|_{\Omega_i}$ is the function value in grid point jh for the function u restricted to cell Ω_i. Point-wise vector grid-functions are obtained by a restriction operator $R_{h,0} : H^2(\mathbb{R}_h) \to [\ell^2(\mathbb{Z}_h)]^4$ defined by

$$\begin{aligned}\mathbf{u}_h(jh) &= (R_{h,0} u)(jh) = \\ &= \begin{bmatrix} -h & u'(jh)|_{\Omega_{j-1}} - u\left((j-1)h\right)|_{\Omega_{j-1}} + u(jh)|_{\Omega_{j-1}} \\ & u(jh)|_{\Omega_{j-1}} \\ & u(jh)|_{\Omega_j} \\ h & u'(jh)|_{\Omega_j} + u(jh)|_{\Omega_j} - u\left((j+1)h\right)|_{\Omega_j} \end{bmatrix}.\end{aligned} \tag{3.6}$$

In both cases the restriction determines the function values and the correction for the derivatives at the cell boundaries. Only the ordering in the vector function is different: the discrete data are either cell-wise or point-wise collected. These two representations correspond with the representations (2.8) and (2.9) of the block Toeplitz matrix obtained for the DG discretisation.

3.2 Fourier analysis for a block Toeplitz operator

For a block Toeplitz matrix of the type as encountered in Section 2.2 we can compute the Fourier transform and the eigenvalues as follows. Let $A_h = (\mathbf{a}_{m,j}) \in \mathbb{R}^{4\mathbb{Z}\times 4\mathbb{Z}}$ be an infinite Toeplitz operator, i.e., an operator with a block structure $\mathbf{a}_{m,j} \in \mathbb{R}^{4\times 4}$, $m, j \in \mathbb{Z}$, satisfying $\mathbf{a}_{m,m+k} = \mathbf{a}_{-k} \quad \forall m, k \in \mathbb{Z}$, and let $e_{h,\omega}$ be an elementary mode, i.e., a complex function defined on the grid $\mathbb{Z}_h$ with $e_{h,\omega}(jh) = e^{ijh\omega}$, then

$$\begin{aligned}&\sum_{j\in\mathbb{Z}} \mathbf{a}_{m,j} e_{h,\omega}(jh) = \widehat{A}_h(\omega) e_{h,\omega}(mh) \Leftrightarrow \\ &\widehat{A}_h(\omega) = \sum_{j\in\mathbb{Z}} \mathbf{a}_{m,j} e^{i(j-m)h\omega} = \sum_{k\in\mathbb{Z}} \mathbf{a}_{-k} e^{ikh\omega} = \sum_{k\in\mathbb{Z}} \mathbf{a}_k e^{-ikh\omega},\end{aligned} \tag{3.7}$$

for all $\omega \in \mathbb{T}_h \equiv [-\frac{\pi}{h}, \frac{\pi}{h}]$.

Now, let $V_h \in \mathbb{R}^{4\mathbb{Z}\times 4\mathbb{Z}}$ be an arbitrary diagonal block-Toeplitz matrix, with blocks $\mathbf{v}_{j,j} = \mathbf{v} \in \mathbb{R}^{4\times 4}$, $\forall j \in \mathbb{Z}$, then

$$\left(A_h V_h e_{h,\omega}\right)(mh) = \sum_{j\in\mathbb{Z}} \mathbf{a}_{m,j}\mathbf{v}_{j,j} e^{ijh\omega} = \left(\sum_{j\in\mathbb{Z}} \mathbf{a}_{m,j} e^{ijh\omega}\right)\mathbf{v} = \widehat{A}_h(\omega) e^{imh\omega}\mathbf{v}\,,$$

with

$$\widehat{A}_h(\omega)\mathbf{v} = \left(\sum_{j\in\mathbb{Z}} \mathbf{a}_j e^{-ijh\omega}\right)\mathbf{v}.$$

If we choose $\mathbf{v} = \mathbf{v}(\omega)$ to be the matrix of eigenvectors of $\widehat{A}_h(\omega)$, such that:

$$\widehat{A}_h(\omega)\mathbf{v} = \mathbf{v}\Lambda_h(\omega), \tag{3.8}$$

then we have:

$$\left(A_h V_h e_{h,\omega}\right)(jh) = \widehat{A}_h(\omega)\mathbf{v} e_{h,\omega}(mh) = e_{h,\omega}(mh)\mathbf{v}\Lambda_h(\omega). \tag{3.9}$$

Hence, the columns of $\mathbf{v}(\omega)e_{h,\omega}(mh)$ are the eigenvectors of A_h. And $\Lambda_h(\omega)$ is a family of 4×4 diagonal matrices with the eigenvalues of A_h at the diagonal entries.

Corollary 1. We readily see that $\widehat{A_h}(\omega)$ satisfies

$$\widehat{A_h\mathbf{u}_h}(\omega) = \widehat{A_h}(\omega)\ \widehat{\mathbf{u}_h}(\omega). \tag{3.10}$$

Corollary 2. The spectrum of the Toeplitz operator A_h is found as $\{\lambda_i(\omega)\}_{i=1,\cdots,4}$, $\omega \in \mathbb{T}_h$, where $\lambda_i(\omega)$ is an eigenvalue of $\widehat{A_h}(\omega)$.

3.3 Fourier analysis for prolongations and restrictions

Key to the Fourier analysis of prolongations and restrictions are the flat prolongation and restriction operators $P^0_{hH} : [\ell^2(\mathbb{Z}_H)]^4 \to [\ell^2(\mathbb{Z}_h)]^4$ and $R^0_{Hh} : \ell^2(\mathbb{Z}_h) \to \ell^2(\mathbb{Z}_H)$, that are defined by

$$\mathbf{u}_h(jh) = \left(P^0_{hH}\mathbf{u}_H\right)(jh) = \begin{cases} \mathbf{u}_H(Hj/2), & \text{if } j \text{ even}, \\ \mathbf{0}, & \text{if } j \text{ odd}, \end{cases} \tag{3.11}$$

and

$$\left(R^0_{Hh}\mathbf{u}_h\right)(jH) = \mathbf{u}_h(2jh). \tag{3.12}$$

General, arbitrary constant coefficient prolongations (restrictions) can be constructed as a combination of a Toeplitz and a flat operator. Any prolongation P_{hH} can be written as $P_{hH} = P_h P^0_{hH}$ and any restriction R_{Hh} as $R_{Hh} = R^0_{Hh}R_h$, with P_h (or R_h) a Toeplitz operator $[\ell^2(\mathbb{Z}_h)]^4 \to [\ell^2(\mathbb{Z}_h)]^4$.

A simple computation [12] shows

$$\widehat{P^0_{hH}\mathbf{u}_H}(\omega) = \frac{1}{2}\widehat{\mathbf{u}_H}(\omega), \quad \omega \in \mathbb{T}_h. \tag{3.13}$$

(notice the periodicity of $\widehat{u_H}(\omega)$ with period π/h !) and

$$\widehat{R^0_{Hh}\mathbf{u}_h}(\omega) = \sum_{p=0,1} \widehat{\mathbf{u}_h}\left(\omega + \frac{\pi p}{h}\right), \quad \forall \omega \in T_H = T_{2h}. \tag{3.14}$$

Here we see that $\widehat{P_{hH}u_H}$ is defined on $\mathbb{T}_h = [-\pi/h, +\pi/h]$, whereas $\widehat{u_H}$ is defined on the smaller $\mathbb{T}_H = [-\pi/2h, \pi/2h]$. This motivates us to introduce a different notation for the same Fourier transform $\widehat{v_h}(\omega)$, with $\omega \in \mathbb{T}_h$. We introduce the new notation

$$\begin{pmatrix} \widehat{v_h}(\omega) \\ \widehat{v_h}(\omega + \pi/h) \end{pmatrix}, \quad \omega \in \mathbb{T}_H \ ,$$

with exactly the same meaning as $\widehat{v_h}$, $\omega \in \mathbb{T}_h$.

Having introduced this notation, we may write (3.13) as

$$\widehat{P_{hH}\mathbf{u}_H}(\omega) = \left(P_h\widehat{P^0_{hH}\mathbf{u}_H}\right)(\omega) = \frac{1}{2}\begin{bmatrix} \widehat{P_h}(\omega) \\ \widehat{P_h}\left(\omega + \frac{\pi}{h}\right) \end{bmatrix} \widehat{\mathbf{u}_h}(\omega), \quad \omega \in \mathbb{T}_H, \tag{3.15}$$

and (3.12) as

$$\widehat{R_{Hh}\mathbf{u}_h}(\omega) = \widehat{R^0_{Hh}R_h}\mathbf{u}_h(\omega) = \begin{bmatrix} \widehat{R_h}(\omega), & \widehat{R_h}\left(\omega + \frac{\pi}{h}\right) \end{bmatrix} \begin{bmatrix} \widehat{\mathbf{u}_h}(\omega) \\ \widehat{\mathbf{u}_h}\left(\omega + \frac{\pi}{h}\right) \end{bmatrix}, \tag{3.16}$$

with $\omega \in \mathbb{T}_H$.

3.4 Filtering the true HF functions

On the one hand we can define low and high frequency grid functions in $\ell^2(\mathbb{Z}_h)$ as the functions that are linear combinations of modes $e^{ijh\omega}$, with respectively $\omega \in \mathbb{T}_{2h}$ and $\omega \in \mathbb{T}_h \setminus \mathbb{T}_{2h}$. On the other hand, having introduced a prolongation P_{hH} and a restriction R_{Hh} in the solution space S_h, we may define low frequency components in the error as those components that lie in the range of the projection $P_{hH}R_{Hh}$, and high frequency components as the complementary functions, i.e., those in the range of $I_h - P_{hH}R_{Hh}$. In view of the multigrid algorithm, the latter approach seems the more relevant.

Since a low frequency grid function can be represented on the coarser grid, we obtain this grid-function by considering a 'slowly varying' (4-valued) gridfunction $\mathbf{u}_h$

$$P_{hH}R_{Hh}\mathbf{u}_h = P_h P^0_{hH} R^0_{Hh} R_h \mathbf{u}_h. \tag{3.17}$$

Since $P_{hH}R_{Hh}$ is a projection we have for a high frequency grid-function $\mathbf{u}_h$:

$$(I - P_h P^0_{hH} R^0_{Hh} R_h)\mathbf{u}_h = \mathbf{u}_h\,. \tag{3.18}$$

In view of this we want that our multigrid smoothers (the relaxation methods) damp the contributions (3.18). In other words: those eigenvalues of the amplification operator M^{REL}_h that correspond with high frequency contributions (3.18) must be small. So we are interested to check if the eigenvalues are small for

$$\mathbf{FT}\left((I - P_h P^0_{hH} R^0_{Hh} R_h)\; M^{\mathrm{REL}}\right)(\omega), \quad \omega \in T_H\,.$$

where **FT** denotes the Fourier transform. In matrix notation: in the light of the prolongation P_{hH} and the restriction R_{Hh} the smoothing qualities of the relaxation are described by the eigenvalues of

$$\left(\begin{pmatrix} I & \\ & I \end{pmatrix} - \frac{1}{2}\begin{pmatrix} \widehat{P_h}(\omega)\widehat{R_h}(\omega) & \widehat{P_h}(\omega)\widehat{R_h}(\omega+\frac{\pi}{h}) \\ \widehat{P_h}(\omega+\frac{\pi}{h})\widehat{R_h}(\omega) & \widehat{P_h}(\omega+\frac{\pi}{h})\widehat{R_h}(\omega+\frac{\pi}{h}) \end{pmatrix}\right) \cdot \begin{pmatrix} \widehat{M^{\mathrm{REL}}}(\omega) & \\ & \widehat{M^{\mathrm{REL}}}(\omega+\frac{\pi}{h}) \end{pmatrix}, \tag{3.19}$$

for $\omega \in \mathbb{T}_H$.

3.5 Fourier transform of the two-level operator

Now, with these tools available, we write for the amplification operator of the coarse-grid correction operator

$$M^{\mathrm{CGC}}_h = I_h - P_{hH} L_H^{-1} \overline{R}_{Hh} L_h$$

its Fourier transform

$$\widehat{M^{\mathrm{CGC}}_h}(\omega) = \left(\widehat{I_h} - \widehat{P_{hH}}\widehat{L_H^{-1}}\widehat{\overline{R}_{Hh}}\widehat{L_h}\right)(\omega) = \begin{pmatrix} 1 & 0 \\ 0 & 1 \end{pmatrix} - \begin{pmatrix} \widehat{P_h}(\omega) \\ \widehat{P_h}(\omega+\pi/h) \end{pmatrix} (\widehat{L_H}(\omega))^{-1} \begin{pmatrix} \widehat{\overline{R}_h}(\omega) & \widehat{\overline{R}_h}(\omega+\pi/h) \end{pmatrix} \begin{pmatrix} \widehat{L_h}(\omega) & 0 \\ 0 & \widehat{L_h}(\omega+\pi/h) \end{pmatrix}.$$

In view of Parseval's equality (3.3) the eigenvalues of the 8×8-matrix $\widehat{M^{\mathrm{CGC}}_h}(\omega)$ for $\omega \in \mathbb{T}_H$ yield the eigenvalues of the coarse-grid correction operator M^{CGC}_h and similarly $\widehat{M^{\mathrm{TLA}}_h}(\omega) = (\widehat{M^{\mathrm{REL}}_h}(\omega))^{\nu_2}\widehat{M^{\mathrm{CGC}}_h}(\omega)(\widehat{M^{\mathrm{REL}}_h}(\omega))^{\nu_1}$ yield the eigenvalues for the two-level operator M^{TLA}_h.

4. Smoothing analysis

One of the main ingredients of a multi-grid solver is the smoother. It is used to damp the high frequencies of the error on the finer grid, while the low frequency errors are damped by the coarse grid correction. For this, the smoother should have an amplification operator with a proper eigenvalue spectrum. That is, an eigenvalue spectrum in which most eigenvalues are in absolute value less than one, where the larger eigenvalues correspond to low frequency eigenfunctions. In this section we apply Fourier analysis to study the amplification operator of the damped block-Jacobi (JOR) and the damped block-Gauss Seidel (DGS) relaxation for both the stencils (2.8) and (2.9). So, we distinguish between cell-wise block and point-wise block relaxations.

We will observe that with cell-wise relaxations the amplification operators have a complex eigenvalue spectrum with many eigenvalues close to one. This indicates that this relaxation shows a poor and oscillating convergence. However, for point-wise block relaxations the amplification operators show much better spectra.

For the discrete system $A_h x = b$ we consider the iterative process

$$x^{(i+1)} = x^{(i)} - B_h(A_h x^{(i)} - b)\,, \tag{4.1}$$

with B_h an approximate inverse of A_h. Decomposing A_h as

$$A_h = L + D + U, \tag{4.2}$$

into a strict block-lower, a block-diagonal and a strict block upper matrix, the different relaxation methods are uniquely described either by B_h or by the amplification matrix $M_h^{\mathrm{REL}} = I_h - B_h A_h$. These operators are shown in Table 1. Because A_h is a block Toeplitz

	B_h	M_h^{REL}
JOR	αD^{-1}	$D^{-1}((1-\alpha)D - \alpha(L+U))$
DGS_L	$\alpha(D+L)^{-1}$	$(D+L)^{-1}((1-\alpha)(D+L) - \alpha U)$
DGS_U	$\alpha(D+U)^{-1}$	$(D+U)^{-1}((1-\alpha)(D+U) - \alpha L)$

Table 1: The relaxation methods used
$\alpha > 0$ is the relaxation parameter.

operator, also the amplification matrix M_h is block Toeplitz. Notice, that the meaning of the block decomposition (4.2) is different for the stencils (2.8) and (2.9). The stencils corresponding with the decomposition $A_h = (\mathbf{a}_{m,j})$ are given in Table 2.

The difference between cell-wise and point-wise block-decomposition is, that the eigenvectors $e_{h,\omega}(mh)\mathbf{v}$ of the cell-wise stencil correspond with 4-valued grid functions associated with the cell interiors (in fact independent of the chosen basis), whereas for the point-wise stencil, they correspond to the 4-valued grid function (3.6) associated with *the nodal points* between the cells. This makes the cell-wise stencil less suited for a multi-grid algorithm, because it is less natural to define prolongations and restrictions for the staggered information than from the pointwise information in coarse and fine cells.

Using (3.7) we find the Fourier transforms of the basic Toeplitz operators:

$$\widehat{L}(\omega) = L\, e^{-i\omega h}, \quad \widehat{D}(\omega) = D, \quad \widehat{U}(\omega) = U\, e^{i\omega h}. \tag{4.3}$$

cell-wise		point-wise
$\begin{bmatrix} -\frac{1}{2} & 0 & -\frac{1}{2} & \frac{1-\sigma}{2} - h\mu \\ 0 & 0 & 0 & \frac{1}{2}\sigma \\ 0 & 0 & 0 & 0 \\ 0 & 0 & 0 & \frac{1}{2}\sigma \end{bmatrix}$	L	$\begin{bmatrix} 0 & 0 & 0 & \frac{1}{30} \\ 0 & \frac{1}{2}\sigma & \frac{-1-\sigma}{2} & 0 \\ 0 & 0 & -\frac{1}{2} & 0 \\ 0 & 0 & 0 & 0 \end{bmatrix}$
$\begin{bmatrix} \frac{1+\sigma}{2} + h\mu & \frac{1}{2} & 0 & \frac{-1-\sigma}{2} \\ -\frac{1}{2}\sigma & \frac{2}{15} & \frac{1}{30} & 0 \\ 0 & \frac{1}{30} & \frac{2}{15} & -\frac{1}{2}\sigma \\ \frac{-1-\sigma}{2} & 0 & \frac{1}{2} & \frac{1+\sigma}{2} + h\mu \end{bmatrix}$	D	$\begin{bmatrix} \frac{2}{15} & -\frac{1}{2}\sigma & \frac{1}{2}\sigma & 0 \\ \frac{1}{2} & \frac{1+\sigma}{2} + h\mu & \frac{1-\sigma}{2} - h\mu & -\frac{1}{2} \\ -\frac{1}{2} & \frac{1-\sigma}{2} - h\mu & \frac{1+\sigma}{2} + h\mu & \frac{1}{2} \\ 0 & \frac{1}{2}\sigma & -\frac{1}{2}\sigma & \frac{2}{15} \end{bmatrix}$
$\begin{bmatrix} \frac{1}{2}\sigma & 0 & 0 & 0 \\ 0 & 0 & 0 & 0 \\ \frac{1}{2}\sigma & 0 & 0 & 0 \\ \frac{1-\sigma}{2} - h\mu & -\frac{1}{2} & 0 & -\frac{1}{2} \end{bmatrix}$	U	$\begin{bmatrix} 0 & 0 & 0 & 0 \\ 0 & -\frac{1}{2} & 0 & 0 \\ 0 & \frac{-1-\sigma}{2} & \frac{1}{2}\sigma & 0 \\ \frac{1}{30} & 0 & 0 & 0 \end{bmatrix}$

Table 2: The stencils in the diagonal decomposition

This yields the Fourier transform for the amplification operators of JOR and DGS:

$$\widehat{M_{JOR}^{REL}} = \widehat{D}^{-1}\left((1-\alpha)\,\widehat{D} - \alpha\,\left(\widehat{L}+\widehat{U}\right)\right),$$

$$\widehat{M_{DGS_L}^{REL}} = \left(\widehat{D}+\widehat{L}\right)^{-1}\left((1-\alpha)\left(\widehat{D}+\widehat{L}\right) - \alpha\,\widehat{U}\right),$$

$$\widehat{M_{DGS_U}^{REL}} = \left(\widehat{D}+\widehat{U}\right)^{-1}\left((1-\alpha)\left(\widehat{D}+\widehat{U}\right) - \alpha\,\widehat{L}\right).$$

Because of (3.9), computing the eigenvalues of $\widehat{M_h^{REL}}(\omega)$ for $\omega \in \mathbb{T}_h$ we find the eigenvalues of M_h^{REL}. The eigenvalues corresponding with the high frequencies (i.e., the frequencies $|\omega| > \pi/2h$, that cannot be represented on the coarser grid) are found as $\widehat{M_h^{REL}}(\omega)$ for $\omega \in \mathbb{T}_h \setminus \mathbb{T}_H$. For the various DG-methods, viz., for Baumann's method, $\sigma = 1$, $\mu = 0$; for the symmetric DG method, $\sigma = -1$, $\mu = 0$; and for the internal penalty DG method (IP-method), $\sigma = -1$, $\mu = C/h$, Figures 2-10 show the eigenvalue spectra of JOR, DGS and symmetric Gauss Seidel $M_{SGS}^{REL} = M_{DGS_L}^{REL} M_{DGS_U}^{REL}$, relaxation amplification operators.

We notice that the spectra of the amplification operators *for point-wise ordering* of the block relaxations appear to be the same for the Baumann and the symmetric DG-method ($\sigma = 1$ or $\sigma = -1$).

Although in these figures we do distinguish between the behavior for low and high frequencies (LF: $|\omega| < \pi/2h$ and HF: $|\omega| \geq \pi/2h$), this does not precisely correspond with the meaning of LF and HF in the context of multigrid. Typical LF components in a multigrid algorithm are those functions that are invariant under the projection $P_{hH}R_{Hh}$; they are in the range of the prolongation, whereas the HF components are those in the kernel of the restriction. Therefore, and to determine optimal relaxation parameters, taking into account the

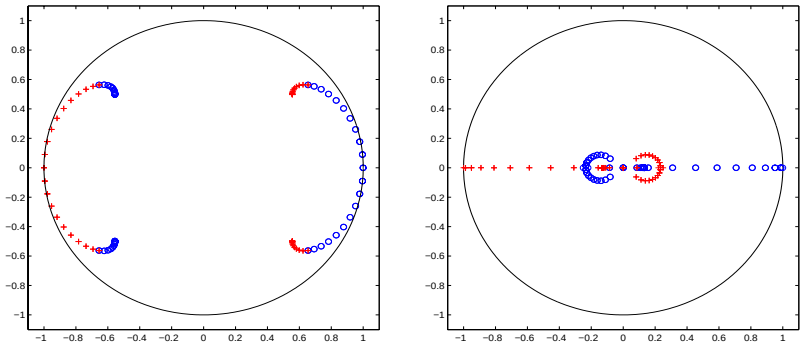

Cell-wise order Point-wise order

$\circ : \omega_{low} \in [-\pi/2h, \pi/2h], \quad + : \omega_{high} \in [-\pi/h, -\pi/2h] \cup [\pi/2h, \pi/h]$

Figure 2: Eigenvalue spectra of $\widehat{M_{JOR}^{REL}(\omega)}$ for Baumann's DG-method (without damping: $\sigma = 1$, $\mu = 0$, $\alpha = 1$), relative to the unit circle.

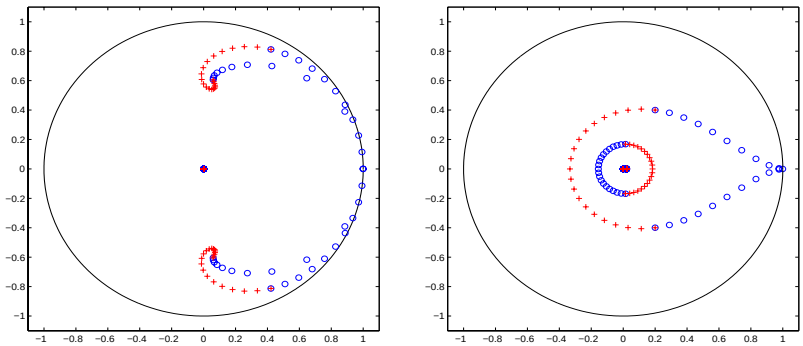

Cell-wise order Point-wise order

$\circ : \omega_{low} \in [-\pi/2h, \pi/2h], \quad + : \omega_{high} \in [-\pi/h, -\pi/2h] \cup [\pi/2h, \pi/h]$

Figure 3: Eigenvalue spectra of $\widehat{M_{DGS}^{REL}(\omega)}$ for Baumann's DG-method (without damping: $\sigma = 1$, $\mu = 0$, $\alpha = 1$), relative to the unit circle.

properties of the restriction and prolongation, we also determine the spectra of the operator $M^{\mathrm{REL}}(I_h - P_{hH}R_{Hh})$.

Because Figures 2-10 show clearly that the convergence behavior of pointwise relaxation is much better than for cellwise relaxation, we further restrict our study to the former.

Figures 11 to 13 show the spectra of the operator $M^{\mathrm{REL}}(I_h - P_{hH}R_{Hh})$, again applied to the three different types of DG-methods. From these results we can determine optimal damping parameters for relaxation. This parameter, minimizing the spectral radius $\rho(M_h^{REL}(I_h - P_{hH}R_{Hh}))$ is given by:

$$\alpha_{opt} = \frac{2}{2 - (\lambda_{\min} + \lambda_{\max})},$$

where $\lambda_{\min}$ and $\lambda_{\max}$ are respectively the minimum and maximum (real) eigenvalues of the spectrum without damping. The damping parameters are given in Table 3. In Table 4 we

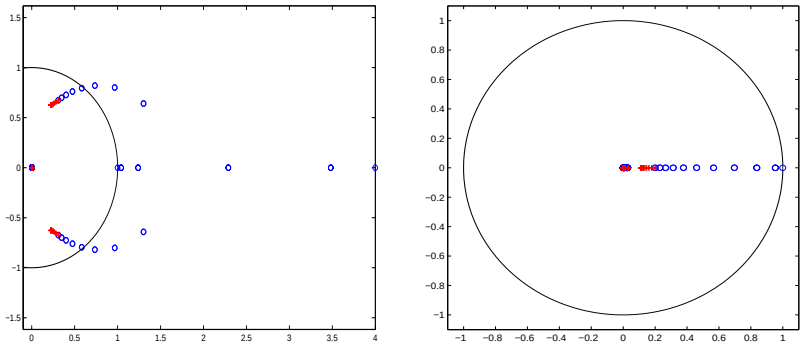

Cell-wise order Point-wise order

$\circ : \omega_{low} \in [-\pi/2h, \pi/2h], \quad + : \omega_{high} \in [-\pi/h, -\pi/2h] \cup [\pi/2h, \pi/h]$

Figure 4: Eigenvalue spectra of $\widehat{M_{SGS}^{REL}(\omega)}$ for Baumann's DG-method (without damping: $\sigma = 1$, $\mu = 0$, $\alpha = 1$), relative to the unit circle.

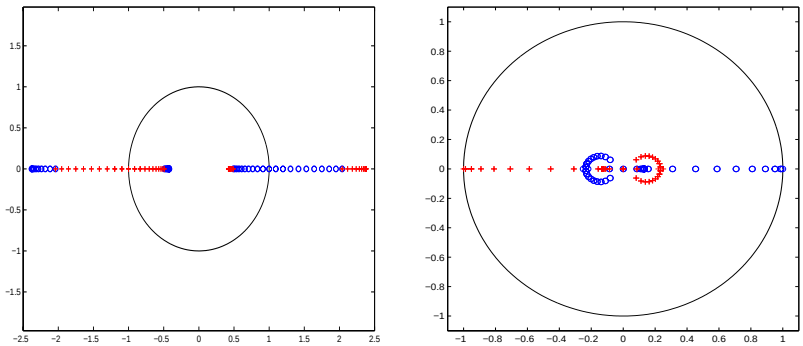

Cell-wise order Point-wise order

$\circ : \omega_{low} \in [-\pi/2h, \pi/2h], \quad + : \omega_{high} \in [-\pi/h, -\pi/2h] \cup [\pi/2h, \pi/h]$

Figure 5: Eigenvalue spectra of $\widehat{M_{JOR}^{REL}(\omega)}$, for symmetric DG-method (without damping: $\sigma = -1$, $\mu = 0$, $\alpha = 1$), relative to the unit circle.

show the spectral radii for the corresponding operators $M_h^{\mathrm{REL}}(I_h - P_{hH}R_{Hh})$. For the spectral radius of symmetric damped Gauss-Seidel the damping parameter for damped Gauss Seidel are used. In the next section we use a similar approach to optimize the two-level algorithm.

5. Two-level analysis

In this section we study the convergence behavior of a two-level algorithm, both for the error and the residue. In a similar fashion as we have determined relaxation parameters for the smoothing operators, we determine optimal relaxation parameters for the two-level operators in order to minimize the spectral radii. The amplification of the error for the two-level algorithm is given by the operator

$$\begin{aligned} M_h^{TLA} &= \left(M_h^{\mathrm{REL}}\right)^{\nu_2} M_h^{\mathrm{CGC}} \left(M_h^{\mathrm{REL}}\right)^{\nu_1} \\ &= \left(M_h^{\mathrm{REL}}\right)^{\nu_2} \left(I - P_{hH} L_H^{-1} \overline{R}_{Hh} L_h\right) \left(M_h^{\mathrm{REL}}\right)^{\nu_1}, \end{aligned}$$

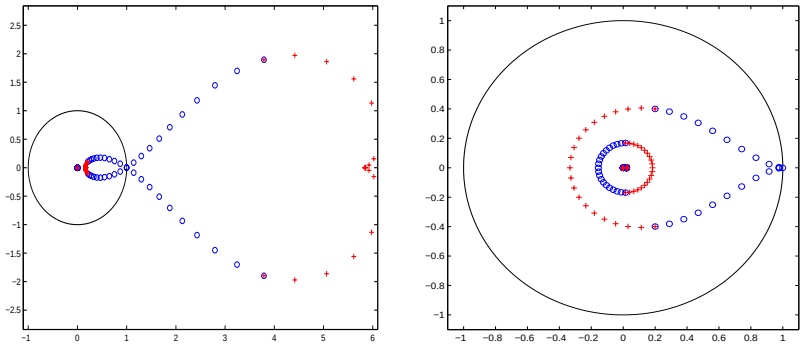

Cell-wise order Point-wise order

$\circ : \omega_{low} \in [-\pi/2h, \pi/2h], \quad + : \omega_{high} \in [-\pi/h, -\pi/2h] \cup [\pi/2h, \pi/h]$

Figure 6: Eigenvalue spectra of $\widehat{M_{DGS}^{REL}}(\omega)$ for the symmetric DG-method (without damping: $\sigma = -1$, $\mu = 0$, $\alpha = 1$), relative to the unit circle.

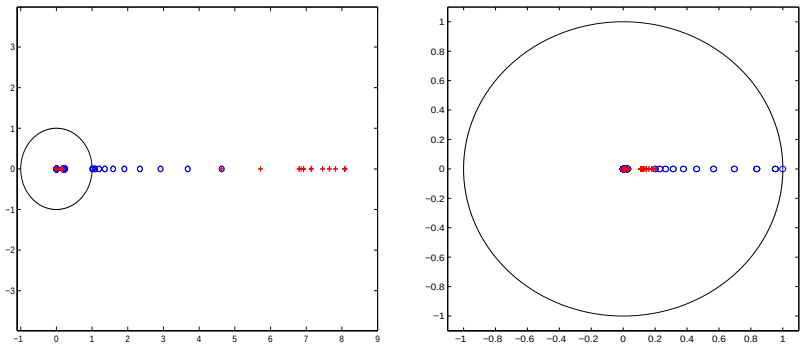

Cell-wise order Point-wise order

$\circ : \omega_{low} \in [-\pi/2h, \pi/2h], \quad + : \omega_{high} \in [-\pi/h, -\pi/2h] \cup [\pi/2h, \pi/h]$

Figure 7: Eigenvalue spectra of $\widehat{M_{SGS}^{REL}}(\omega)$ for the symmetric DG-method (without damping: $\sigma = -1$, $\mu = 0$, $\alpha = 1$), relative to the unit circle.

where ν_1 and ν_2 are the number of pre- (post-) relaxation sweeps respectively, and M_h^{CGC} is the amplification operator of the coarse grid correction. The amplification operator for the residue is

$$\begin{aligned} \overline{M}_h^{TLA} &= (\overline{M}_h^{REL})^{\nu_2}\, \overline{M}_h^{CGC}\, (\overline{M}_h^{REL})^{\nu_1} \\ &= \left(L_h M_h^{\mathrm{REL}} L_h^{-1}\right)^{\nu_2} L_h M_h^{\mathrm{CGC}} L_h^{-1} \left(L_h M_h^{\mathrm{REL}} L_h^{-1}\right)^{\nu_1}. \end{aligned}$$

In Section 2.3 we already noticed the Galerkin relation (2.10) between the discretisation on the finer and the coarser grid, and that, because test and trial space are the same, the residual restriction $\overline{R}_{Hh}$ is given by $\overline{R}_{Hh} = P_{hH}^T$, i.e. the adjoint of the prolongation. The consequence is that $M_h^{CGC} P_{hH} = 0$ for the solution and that $\overline{R}_{Hh} \overline{M}_h^{CGC} = 0$ for the residue. With the tools developed in the previous sections we now study the eigenvalue spectra of the two-level operators and their spectral norms.

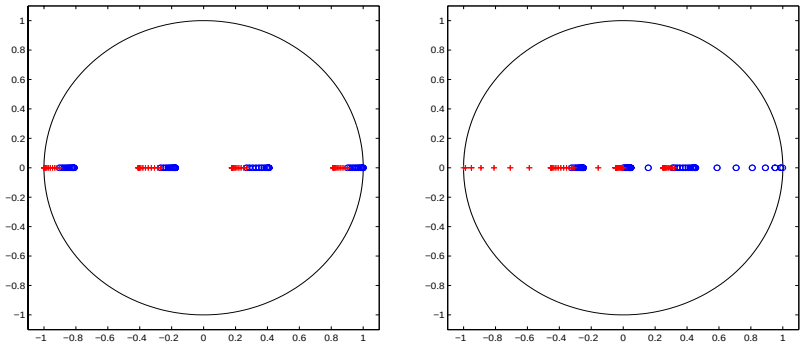

Cell-wise order Point-wise order

$\circ : \omega_{low} \in [-\pi/2h, \pi/2h]$, $+ : \omega_{high} \in [-\pi/h, -\pi/2h] \cup [\pi/2h, \pi/h]$

Figure 8: Eigenvalue spectra of $\widehat{M_{JOR}^{REL}(\omega)}$ for the IP-method (without damping: $\sigma = -1$, $\mu = 10/h$, $\alpha = 1$), relative to the unit circle.

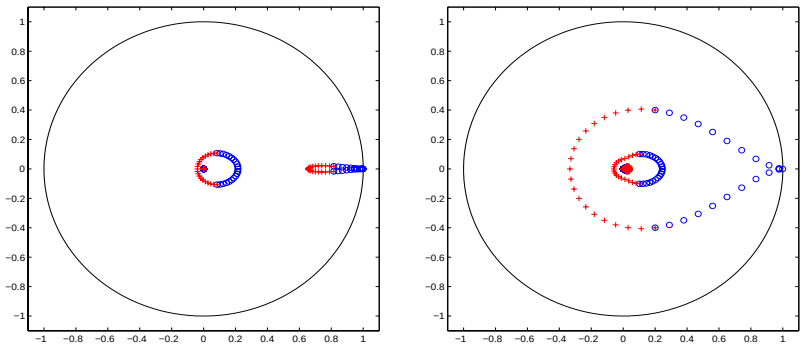

Cell-wise order Point-wise order

$\circ : \omega_{low} \in [-\pi/2h, \pi/2h]$, $+ : \omega_{high} \in [-\pi/h, -\pi/2h] \cup [\pi/2h, \pi/h]$.

Figure 9: Eigenvalue spectra of $\widehat{M_{DGS}^{REL}(\omega)}$ for the IP-method (without damping: $\sigma = -1$, $\mu = 10/h$, $\alpha = 1$), relative to the unit circle.

5.1 Spectrum of the two-level iteration operator

The difference between the coarse grid correction on the error and that on the residue is that the former splits a HF-error mode into an HF- and LF-mode on the finer grid. This, in contrast to the coarse grid correction on the residue, in which a LF-residual mode is split into a HF- and LF-mode on the finer grid [14].

This implies that if we are interested in the error reduction, we should apply the smoothing operator M_h^{REL} *before* the coarse grid correction. On the other hand, if we are interested in residue reduction we should apply the smoothing after the coarse grid correction operator $\overline{M}_h^{CGC}$. Therefore, for the error we are particularly interested in the behavior of the spectrum and the two-norm of

$$M_h^{\mathrm{CGC}} M_h^{\mathrm{REL}} = \left(I - P_{hH} L_H^{-1} \overline{R}_{Hh} L_h\right) M_h^{\mathrm{REL}},$$

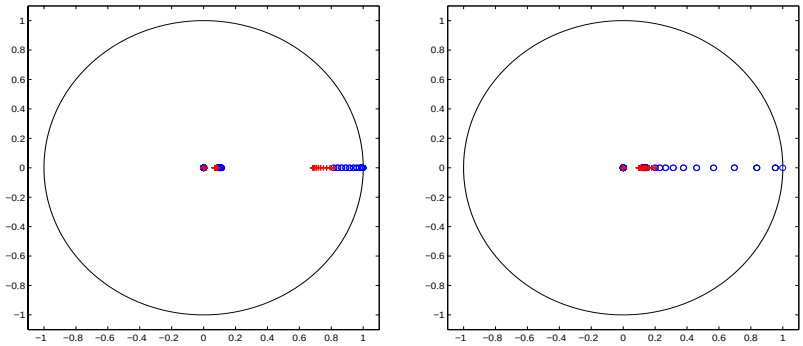

Cell-wise order Point-wise order

$\circ : \omega_{low} \in [-\pi/2h, \pi/2h]$, $+ : \omega_{high} \in [-\pi/h, -\pi/2h] \cup [\pi/2h, \pi/h]$

Figure 10: Eigenvalue spectra of $\widehat{M_{SGS}^{REL}}(\omega)$ for the IP-method (without damping: $\sigma = -1$, $\mu = 10/h$, $\alpha = 1$), relative to the unit circle.

α	Baumann/symmetric DG	symmetric penalized DG
JOR	8/11	0.773
DGS	15/16	1.024

Table 3: Damping parameters for the relaxation.

whereas for the residue we want to study

$$\overline{M}_h^{REL}\,\overline{M}_h^{CGC} = \left(L_h M_h^{\mathrm{REL}} L_h^{-1}\right)\left(I - L_h P_{hH} L_H^{-1} \overline{R}_{Hh}\right).$$

It is clear the the spectra of these operators are the same, but the norms may be different. For different types of DG-methods, viz. for Baumann's method ($\sigma = 1$, $\mu = 0$), the symmetric DG method ($\sigma = -1$, $\mu = 0$), and for the internal penalty method ($\sigma = -1$, $\mu = C/h$), the spectra of the two-level operators can be studied as we did in Section 4 for the smoothing operators, and optimal damping factors can be computed. These damping parameters are given in Table 5. The spectral radii of the two-level operators are shown in Table 6.

We see that the two-level amplification operators for the symmetric-DG method have the smallest spectral radii, which indicates that the final convergence rate will be faster, compared with the Baumann and IP-DG methods.

$\rho(M^{REL}(I_h - P_{hH}R_{Hh}))$	Baumann/symmetric DG	symmetric penalized DG
JOR	0.455	0.591
DGS	0.250	0.365
symm-DGS	0.203	0.200

Table 4: Spectral radii of $M^{REL}(I_h - P_{hH}R_{Hh})$ for damping parameters as in Table 3.

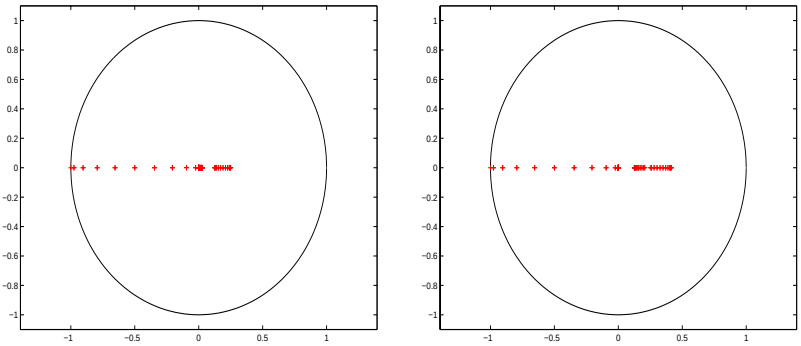

Baumann/symmetric DG penalized symmetric DG

Figure 11: Eigenvalue spectra of $\mathbf{FT}(M_{JOR}^{REL}(I_h - P_{hH}R_{Hh}))(\omega)$ without damping ($\alpha = 1$).

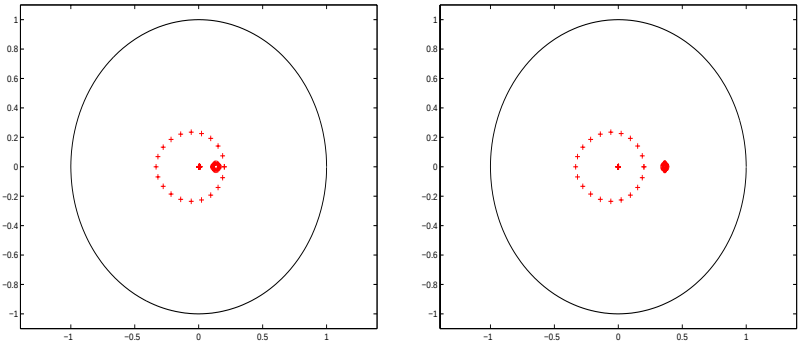

Baumann/symmetric DG penalized symmetric DG

Figure 12: Eigenvalue spectra of $\mathbf{FT}(M_{DGS}^{REL}(I_h - P_{hH}R_{Hh}))(\omega)$ without damping ($\alpha = 1$).

5.2 Spectral norm of the iteration operator for the error and residue

From Section 5.1 we know that all two-level algorithms will converge rapidly after a sufficient number of iterations. However, since we want to minimize the total amount of iteration sweeps, we need to be sure that also the spectral norms of the iteration operators are sufficiently small. In order to check this we apply the singular value decomposition (SVD) to the Fourier transform of the amplification operators,

$$\mathbf{FT}\left(\left(M_h^{\mathrm{TLA}}\right)^t\right)(\omega) = U(\omega)\Sigma(\omega)V^T(\omega), \tag{5.1}$$

α_{opt}	Baum-DG	symm-DG	IP-DG ($\mu = 10/h$)
$M_h^{CGC}M_{JOR}^{REL}$	0.974	0.914	0.989
$M_h^{CGC}M_{DGS}^{REL}$	1.084	0.983	1.078

Table 5: Damping parameters for the two-level operators ($\rho(M_h^{CGC}M_h^{REL}) = \rho(\overline{M}_h^{REL}\overline{M}_h^{CGC})$).

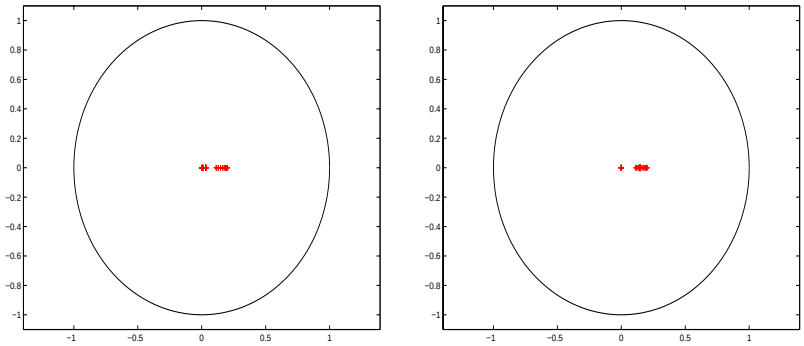

Baumann/symmetric DG penalized symmetric DG

Figure 13: Eigenvalue spectra of $\mathbf{FT}(M^{REL}_{DGS_U}(I_h - P_{hH}R_{Hh})M^{REL}_{DGS_L})(\omega)$ without damping ($\alpha = 1$).

$\rho(M_h^{CGC}M_h^{REL})$	Baum-DG	symm-DG	IP-DG ($\mu = 10/h$)
$M_h^{CGC}M_{JOR}^{REL}$	0.401	0.314	0.422
$M_h^{CGC}M_{DGS}^{REL}$	0.220	0.143	0.189
$M_{DGS_U}^{REL}M_h^{CGC}M_{DGS_L}^{REL}$	0.119	0.073	0.139

Table 6: Spectral radii $\rho(M_h^{CGC}M_h^{REL}) = \rho(\overline{M}_h^{REL}\overline{M}_h^{CGC})$ for damping parameters as in Table 5.

where, in view of our function basis, $U(\omega)$ and $V(\omega)$ are 8×8 unitary matrices and $\Sigma(\omega)$ is a real 8×8 diagonal matrix with singular values. The number of iterations is denoted by t. So, if we consider the error of the approximation, then according to (5.1), this error is first expressed on the basis $V(\omega)$, damped/amplified by $\Sigma(\omega)$ and then transformed to the basis $U(\omega)$. Since the spectral norm of the operator is the maximum singular value, this norm tells us how well the error (c.q. the residue) is damped after t sweeps. The column of $V(\omega)$ determines the corresponding error /residual component.

The spectral norm after one iteration of the optimized two-level operators on the residue for the different types of DG-methods are shown in Table 7. We see that not all two-level operators immediately converge. However, the situation changes if we look at the spectral norm of the two-level operators after 2 iterations (see Table 8). Then all methods converge, even by a significant factor. The spectral norms of the iteration operators on the error are the same as for the residual, except for Baumann's DG method. For this method the error-amplification norm becomes even unbounded (for vanishing frequency ω). This is related to the lack of adjoint consistenct as signaled in [3]. We show the singular values of $\widehat{M_h^{\mathrm{TLA}}}(\omega)$ and $\widehat{\overline{M}_h^{\mathrm{TLA}}}(\omega)$ in the Figures 15 – 17. We see that (as expected) in all cases 4 singular values vanish and that all singular values (except for $\widehat{M_h^{\mathrm{TLA}}}(\omega)$ for Baumann's method) are much smaller than one.

	$\overline{M}_h^{CGC}\overline{M}_{JOR}^{REL}$	$\overline{M}_h^{CGC}\overline{M}_{DGS}^{REL}$	$\overline{M}_{DGS_U}^{REL}\overline{M}_h^{CGC}\overline{M}_{DGS_L}^{REL}$
Baum-DG	1.762	1.364	0.557
Symm-DG	1.282	0.506	0.104
IP-DG ($\mu = 10/h$)	1.518	0.699	0.301

Table 7: The spectral norm ($\sigma_{\max}$) after 1 iteration for the residue with optimal damping.

	$\overline{M}_h^{CGC}\overline{M}_{JOR}^{REL}$	$\overline{M}_h^{CGC}\overline{M}_{DGS}^{REL}$	$\overline{M}_{DGS_U}^{REL}\overline{M}_h^{CGC}\overline{M}_{DGS_L}^{REL}$
Baum-DG	0.684	0.447	0.064
Symm-DG	0.403	0.083	0.007
IP-DG ($\mu = 10/h$)	0.640	0.284	0.038

Table 8: The spectral norm ($\sigma_{\max}$) after 2 iterations for the residue with optimal damping.

6. Galerkin relation and consistency

By the nature of the discontinuous Galerkin method, it is clear that the Galerkin relation,

$$L_H = \overline{R}_{Hh} L_h P_{hH} \,,$$

exists between the discrete operators on the fine and the coarse grid, provided that $\overline{R}_{Hh} = P_{hH}^T$ and that P_{hH} satisfies the requirement that $\mathbf{u}_h$ and $P_{hH}\mathbf{u}_H$ represent the same piecewise polynomial. For the prolongation introduced in Section 2.3 this holds true by construction.

The Galerkin relation, the order of consistency and the order of convergence are easily verified by Fourier analysis. In order to see this in detail and to compute the corresponding order constants, we show some results of this analysis. It also yields some additional insight with respect to the lack of adjoint consistency of Baumann's method (see [3]).

For the analysis we use the four functions in the basis (2.6) with $p = 2$, and consider the related point-wise stencil (2.9). First we are interested in the truncation error operator

$$\tau_h = L_h R_h - \overline{R}_h L, \tag{6.1}$$

and the operator corresponding with the discrete convergence, $C_h = L_h^{-1}\tau_h$. In (6.1) $R_h : C^1(\Omega_h) \to \mathbb{R}^{4\mathbb{Z}_h}$ is the injective restriction similar to (3.6), whereas the second restriction is the Galerkin restriction $\overline{R}_h : C^1(\Omega_h) \to \mathbb{R}^{4\mathbb{Z}_h}$, defined such that for all $f \in C^1(\Omega_h)$,

$$\left(\overline{R}_h f\right)(jh) = \begin{bmatrix} \int_{(j-1)h}^{jh} \phi_k(x) f(x) dx, & k \in \{1,2\}\,, \\ \int_{jh}^{(j+1)h} \phi_k(x) f(x) dx, & k \in \{3,4\}\,, \end{bmatrix}$$

where ϕ_k are the basis functions in point-wise ordering. With $P_h : \mathbb{R}^{4\mathbb{Z}_h} \to \mathrm{Span}(\phi_{j,e}) \subset C^1(\Omega_h)$ the interpolation with $R_h P_h = I_h$, it is clear that, by construction, $P_h = P_{hH} P_H$ and $\overline{R}_H = \overline{R}_{Hh}\overline{R}_h$, and the discrete operator is characterized by $L_h = \overline{R}_h L P_h$. Hence, $L_H = \overline{R}_H L P_H = \overline{R}_{Hh}\overline{R}_h L P_h P_{hH} = \overline{R}_{Hh} L_h P_{hH}$. Furthermore, we write for the truncation error:

$$\tau_h e^{i\omega x} = \tau_h e_\omega(x) = (L_h R_h e_\omega - \overline{R}_h L e_\omega)(x).$$

Baumann	symmetric	IP
$\sigma = 1$ $\mu = 0$	$\sigma = -1$ $\mu = 0$	$\sigma = -1$ $\mu = 1/h$
$\begin{pmatrix} \frac{1}{120}h^4\omega^4 + O(h^5\omega^5) \\ \frac{1}{840}h^4\omega^4 + O(h^5\omega^5) \\ \frac{1}{840}h^4\omega^4 + O(h^5\omega^5) \\ \frac{1}{120}h^4\omega^4 + O(h^5\omega^5) \end{pmatrix}$	$\begin{pmatrix} \frac{1}{120}h^4\omega^4 + O(h^5\omega^5) \\ \frac{1}{3360}h^5\omega^5 + O(h^6\omega^6) \\ \frac{1}{3360}h^5\omega^5 + O(h^6\omega^6) \\ \frac{1}{120}h^4\omega^4 + O(h^5\omega^5) \end{pmatrix}$	$\begin{pmatrix} \frac{1}{120}h^4\omega^4 + O(h^5\omega^5) \\ \frac{1}{2800}h^5\omega^5 + O(h^6\omega^6) \\ \frac{1}{2800}h^5\omega^5 + O(h^6\omega^6) \\ \frac{1}{120}h^4\omega^4 + O(h^5\omega^5) \end{pmatrix}$

Table 9: The expansion of (6.4) for $\omega h \to 0$, i.e., the order of convergence: pointwise values ($\widehat{v}_2$ and $\widehat{v}_3$) and pointwise derivatives ($\widehat{v}_1$ and $\widehat{v}_4$) at the nodal points.

Using (3.6) and the definition of $\overline{R}_h$, we find:

$$\tau_h e_\omega = L_h e^{i\omega jh} \begin{bmatrix} 1 - e^{-i\omega h} - i\omega h \\ 1 \\ 1 \\ 1 - e^{i\omega h} + i\omega h \end{bmatrix} - \omega^2 h e^{i\omega jh} \begin{bmatrix} \int_0^1 e^{i\omega h(t-1)} t^2(1-t)dt \\ \int_0^1 e^{i\omega h(t-1)} t dt \\ \int_0^1 e^{i\omega ht}(1-t)dt \\ \int_0^1 e^{i\omega ht} t(1-t)^2 dt \end{bmatrix},$$

where the basis functions are scaled to the master element $\widehat{\Omega} = [0, 1]$. Hence,

$$\begin{aligned} \tau_h e_\omega &= \left(\widehat{L_h}(\omega) \begin{bmatrix} 1 - e^{-i\omega h} - i\omega h \\ 1 \\ 1 \\ 1 - e^{i\omega h} + i\omega h \end{bmatrix} - \omega^2 h \begin{bmatrix} \int_0^1 e^{i\omega h(t-1)} t^2(1-t)dt \\ \int_0^1 e^{i\omega h(t-1)} t dt \\ \int_0^1 e^{i\omega ht}(1-t)dt \\ \int_0^1 e^{i\omega ht} t(1-t)^2 dt \end{bmatrix} \right) e^{i\omega jh} \\ &= \left(\widehat{L_h}(\omega)\widehat{R_h}(\omega) - \widehat{\overline{R}}_h(\omega)\widehat{L}(\omega) \right) e^{i\omega jh}, \end{aligned} \tag{6.2}$$

where $\widehat{L_h}(\omega)$ is the Fourier transform of the block Toeplitz matrix L_h. Now we find the expansion of the truncation error for $h \to 0$ from (6.2). Both for Baumann's method ($\sigma = 1, \mu = 0$), and for the symmetric DG-method without penalty ($\sigma = -1, \mu = 0$) and with interior penalty ($\sigma = -1, \mu = 1/h$), (the absolute value of) the truncation error is

$$\tau e_\omega = \begin{bmatrix} \frac{1}{720}h^3\omega^4 + O(h^4\omega^5) \\ 0 \\ 0 \\ \frac{1}{720}h^3\omega^4 + O(h^4\omega^5) \end{bmatrix}. \tag{6.3}$$

Notice the factor h^{d-2} involved, with $d = 1$ the dimension of Ω. Similarly, we study the discrete convergence (where no such factor exists) by

$$C_h\, e_\omega = L_h^{-1} \tau_h\, e_\omega = \widehat{L_h}^{-1}(\omega) \left(\widehat{L_h}(\omega)\widehat{R_h}(\omega) - \widehat{\overline{R}_h}(\omega)\widehat{L}(\omega) \right) e^{i\omega jh}. \tag{6.4}$$

The results for the different methods are given in Table 9. We see that the symmetric DG-methods, with and without interior penalty, are more accurate with respect to the pointwise function values than Baumann's method. However, there is no difference in the order of accuracy with respect to the pointwise derivatives.

7. Numerical results

In this section we show by numerical experiments the convergence behavior of the two-level iteration operator for the error with the Baumann and the symmetric DG-method, for the smoothers JOR, DGS and symmetric DGS with the optimal damping parameters. For this purpose we solve Poisson's equation

$$-u_{xx} = \frac{e^{x/\epsilon}}{\epsilon^2(\epsilon^{1/\epsilon}-1)} \text{ with } u(0)=0,\ u(1)=0,$$

which has a solution with a boundary layer of thickness $O(\epsilon)$. To obtain the discrete system we use the fourth order polynomial basis (1) and we set the mesh width $h = 2^{-N}$. We start with an initial function $u_h^0 = u_{h,\mathrm{PRE}}^0$ on the finer grid. We apply ν_1 pre-relaxation sweeps

$$u_{h,\mathrm{PRE}}^{i+1} = u_{h,\mathrm{PRE}}^{i} + B_h\left(f_h - L_h u_{h,\mathrm{PRE}}^{i}\right),$$

where B_h is an approximate inverse of L_h as given in Table 1. We update the solution by a coarse grid correction step, solving the problem once on grid $H = 2^{1-N}$,

$$u_{h,\mathrm{POST}}^{0} = u_{h,\mathrm{PRE}}^{\nu_1} + P_{hH} L_H^{-1} \overline{R}_{Hh}(f_h - L_h u_{h,\mathrm{PRE}}^{\nu_1}),$$

and eventually we apply ν_2 post-relaxations sweeps

$$u_{h,\mathrm{POST}}^{i+1} = u_{h,\mathrm{POST}}^{i} + B_h(f_h - L_h u_{h,\mathrm{POST}}^{i}),$$

to compute $u_h^{i+1} = u_{h,\mathrm{PRE}}^0 = u_{h,\mathrm{POST}}^{\nu_2}$. For the initial function u_h^0 we choose $u_h^0 = R_h u_0 = R_h \sin(2\pi/h)$. To show the convergence of the different methods we measure the residue in the vector norm (3.4). Hence we write

$$\|d_h\|_2 = \|f_h - L_h u_h\|_2 = \left(\sum_{e=1}^{64}\sum_{j=1}^{4} d_{he,j}^2\right)^{\frac{1}{2}},$$

Since the spectral radii of the two-level operators for the Baumann and symmetric DG-method calculated by Fourier analysis are smaller than those of the IP DG-method we only show results for the first two methods. The convergence of the residue for the two-level operator with different smoothers are shown in Figure 14.

We observe that both DG-methods methods show immediately convergence, starting from the first iteration sweep. We see from Figure 14 and Table 10 that the spectral radii obtained from the numerical experiments coincide very well with spectral radii obtained by Fourier analysis (Table 6). We further remark that the symmetric DG-method converges somewhat faster than Baumann's DG-method. In spite of the phenomenon related with the lack of adjoint consistency of Baumann's method, the observed convergence of the error shows in practice the same behavior as the convergence of the residual.

8. Conclusion

In this paper we analyze the convergence of the multigrid algorithm for various discontinuous Galerkin (DG) methods. For convenience we restrict ourselves only to the one-dimensional

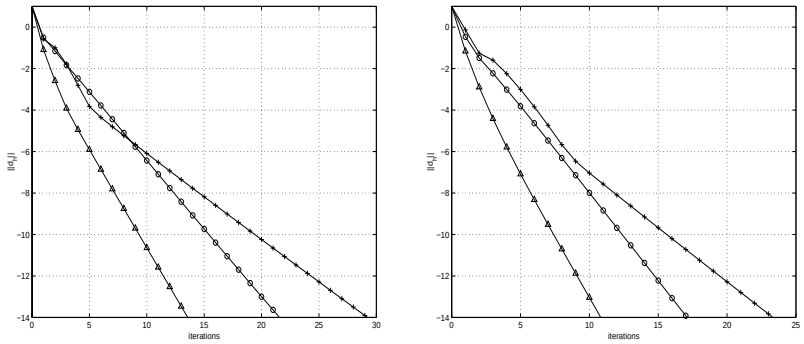

Baumann-DG Symmetric-DG
+: JOR; ∘: DGS; △: SGS.

Figure 14: $\log(||d_h||_2)$ as function of iterations for the two-level iteration operator on the error

$\rho(M_h^{CGC} M_h^{REL})$	Baum-DG	symm-DG
$M_h^{CGC} M_{JOR}^{REL}$	0.38	0.30
$M_h^{CGC} M_{DGS}^{REL}$	0.22	0.14
$M_{DGS_U}^{REL} M_h^{CGC} M_{DGS_L}^{REL}$	0.11	0.07

Table 10: Numerically obtained convergence factors corresponding with $\rho(M_h^{CGC} M_h^{REL}) = \rho(\overline{M}_h^{REL} \overline{M}_h^{CGC})$ for damping parameters as in Table 5.

Poisson problem. We consider the (asymmetric) Baumann-Oden discretisation and the symmetric DG discretisation, with and without interior penalty.

By the choice of a suitable basis in the space of the discontinuous piecewise polynomials that are used for the trial and test space, we are able to introduce a point-wise block partitioning of the discrete operators. It appears that block-relaxation methods based on this pointwise partitioning show completely different convergence properties from those found with classical, cell-wise partitionings. Pointwise block relaxations have much better convergence and smoothing properties. This is most significant for the symmetric DG discretisation without interior penalty. Here, cellwise block-Jacobi or block-Gauss-Seidel relaxation diverge, whereas the pointwise block-relaxations converge.

For the three discretisation methods studied we compute optimal damping parameters for the Jacobi, Gauss-Seidel and symmetric Gauss-Seidel relaxation. The resulting smoothing factors lie between 0.6 (JOR for IP discretisation) and 0.2 (symmetric DG). A two-level analysis with optimal damping parameter shows even better convergence: with spectral radius from 0.4 (JOR for IP discretisation) to 0.075 (for SGS and symmetric DG). An analysis of the spectral norm of the two-level amplification for the residue shows that, a couple (≈ 2) of iteration steps are indeed sufficient to reduce the error by an order of magnitude.

The lack of adjoint consistency of Baumann's method and the resulting loss of accuracy for the solution (and *not* for its derivative) could be analyzed by means of Fourier analysis, and it was also reflected in the spectral norm of the two-level amplification operator for the

error.

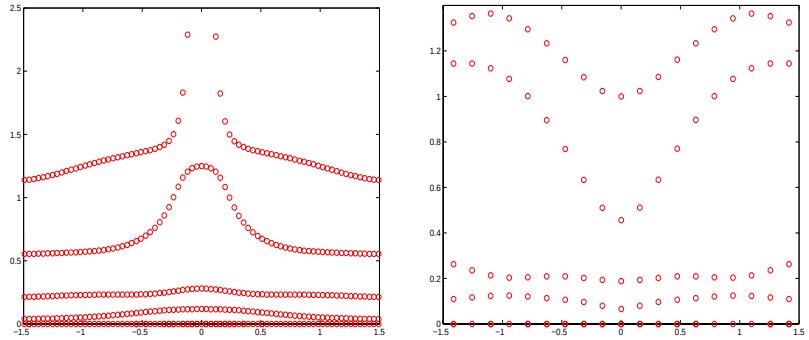

Baumann,$\widehat{M_h^{\mathrm{TLA}}}(\omega)$ Baumann,$\widehat{\overline{M}_h^{\mathrm{TLA}}}(\omega)$

Figure 15: Singular values $\Sigma(\omega)$, $\omega \in [-\pi/2, \pi/2]$, for a TLA-iteration operator: $\widehat{M_h^{\mathrm{TLA}}}(\omega) = \widehat{M_h^{\mathrm{CGC}}}(\omega)\widehat{M_{\mathrm{DGS}}^{\mathrm{REL}}}(\omega)$ and $\widehat{\overline{M}_h^{\mathrm{TLA}}}(\omega) = \widehat{M_{\mathrm{DGS}}^{\mathrm{REL}}}(\omega)\widehat{\overline{M}_h^{\mathrm{CGC}}}(\omega)$.

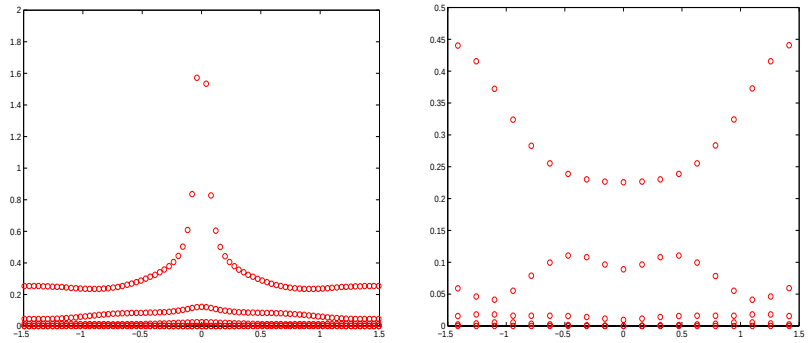

Baumann, $\left(\widehat{M_h^{\mathrm{TLA}}}\right)^2(\omega)$ Baumann, $\left(\widehat{\overline{M}_h^{\mathrm{TLA}}}\right)^2(\omega)$

Figure 16: Singular values $\Sigma(\omega)$, $\omega \in [-\pi/2, \pi/2]$, for two steps of the TLA-iteration operator.

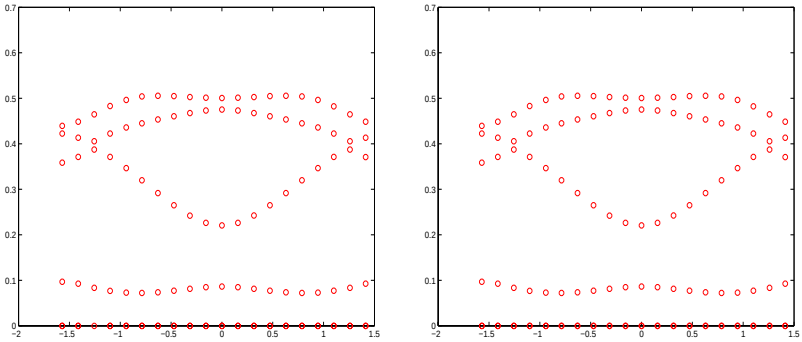

Symmetric DG, $\widehat{M_h^{\mathrm{TLA}}}(\omega)$ Symmetric DG, $\widehat{\overline{M}_h^{\mathrm{TLA}}}(\omega)$

Figure 17: Singular values $\Sigma(\omega)$, $\omega \in [-\pi/2, \pi/2]$, for one step of the symmetric DG TLA-iteration operator.

References

1. I. Abramowitz and I. A. Stegun. *Handbook of Mathematical Functions*. National Bureau of Standards, 1964. (Reprint: Dover Publications Inc.).
2. D. N. Arnold. An interior penalty finite element method with discontinuous elements. *SIAM J. Numer. Anal.*, 19:742–760, 1982.
3. D.N. Arnold, F. Brezzi, B. Cockburn, and D. Marini. Unified analysis of discontinuous Galerkin methods for elliptic problems. *SIAM J Numer. Anal.*, 39:1749–1779, 2002.
4. C. E. Baumann and J. T. Oden. An hp-adaptive discontinuous finite element method for computational fluid dynamics. *The university of Texas at Austin*, 1997.
5. C. E. Baumann and J. T. Oden. A discontinuous *hp* finite element method for convection-diffusion problems. *Comput. Methods Appl. Mech. Engrg.*, 175:311–341, 1999.
6. C.E. Baumann. *An hp-adaptive discontinuous finite element method for computational fluid dynamics*. PhD thesis, The Universitv of Texas at Austin, 1997.
7. A. Brandt. Multi-level adaptive techniques (MLAT) for singular perturbation-problems. In P.W. Hemker and J.J.H. Miller, editors, *Numerical Analysis of Singular Perturbation Problems*, pages 53–142. Academic Press, 1979.
8. B. Cockburn. Discontinuous Galerkin methods for convection-dominated problems. In T. Barth and H. Deconink, editors, *High-Order Methods for Computational Physics*, volume 9 of *Lecture Notes in Comput. Sci. Engrg*, pages 69–224. Springer-Verlag, New York, 1999.
9. L. Delves and C. Hall. An implicit matching principle for global element calculations. *J. Inst. Math. Appl.*, 23:223–234, 1979.
10. J. Gopalakrishnan and G. Kanschat. A multilevel discontinuous Galerkin method. *Numer. Math.*, 2002. to appear.
11. W. Hackbusch. *Multigrid Methods and Applications*. Springer Verlag, 1985.
12. P. W. Hemker. Fourier analysis of gridfunctions, prolongations and restrictions. Technical

Report NW 93, Mathematical Centre, Amsterdam, 1980.

13. P. W. Hemker. On the structure of an adaptive multi-level algorithm. *BIT*, 20:289–301, 1980.
14. P. W. Hemker. A note on defect correction processes with an approximate inverse of deficient rank. *Appl. Math. Comp.*, 8:137–139, 1982.
15. P. Houston, C. Schwab, and E. Süli. Discontinuous *hp*-finite element methods for advection-diffusion problems. Technical Report No. 2000-07, ETHZ, Zürich, Switzerland, 2000.
16. C. Johnson and J. Pitkäranta. An analysis of the discontinuous Galerkin method for a scalar hyperbolic equation. *Mathematics of Computation*, 46:1–26, 1986.
17. J. A. Nitsche. Über ein Variationsprinzip zur Lösung Dirichlet-Problemen bei Verwendung von Teilräumen, die keinen Randbedingungen unterworfen sind. *Abh. Math. Sem. Univ. Hamburg*, 36:9–15, 1971.
18. J.T. Oden, I. Babuška, and C.E. Baumann. A discontinuous *hp* finite element method for diffusion problems. *J. Comp. Phys.*, 146:491–519, 1998.
19. W. H. Reed and T. R. Hill. Triangular mesh methods for the neutron transport equation. Technical Report LA-UR-73-479, Los Alamos Scientific Laboratory, Los Alamos, NM, 1973.
20. B. Rivière, M. F. Wheeler, and V. Girault. Improved energy estimates for interior penalty, cpnstrained and discontinuous Galerkin methods for elliptic problems. Part I. *Computational Geosciences*, 3:337–360, 1999.
21. E. Süli, C. Schwab, and P. Houston. *hp*-DGFEM for partial differential equations with non-negative characteristic form. In B. Cockburn, G. E. Karniadakis, and C.-W. Shu, editors, *Discontinuous Galerkin Methods. Theory, Computation and Applications*, volume 11 of *Lecture Notes in Comput. Sci. Engrg.*, pages 221–230. Springer-Verlag, New York, 2000.
22. M. F. Wheeler. An elliptic collocation-finite element method with interior penalties. *SIAM J. Numer. Anal.*, 15:152–161, 1978.